Rev. Roum. Sci. Techn.– Électrotechn. et Énerg.
Vol. **68**, *1*, pp. 58–64, Bucarest, 2023

IMPROVED ADAPTIVE NONLINEAR CONTROL FOR VARIABLE SPEED WIND-TURBINE FED BY DIRECT MATRIX CONVERTER

FAYSSAL AMRANE [*, 1, 3], AZEDDINE CHAIBA [1, 2], BRUNO FRANCOIS [3]

Keywords: Input-output linearizing and decoupling control (I/OLDC); Doubly fed induction generator (DFIG); Matrix converter (MC); Wind energy conversion system (WECS); Model reference adaptive control (MRAC).

This paper proposes a robust decoupling power algorithm based on a doubly fed induction generator (DFIG) for variable speed wind-turbine (WT). The DFIG rotor circuit is fed by the direct matrix converter (DMC), which presents several features such as no need to the dc-bus voltage, sinusoidal supply, rotor side waveforms, bidirectional power flow, and adjustable input power factor. The 18 bidirectional switches are controlled using the Venturini modulation technique. On the other hand, the DFIG stator circuit is connected directly to the grid. The nonlinear control strategy based on feedback linearization is applied to control the stator power (Ps and Qs) independently using the rotor quadrature and direct currents (irq and ird), which present the images of the previous stator powers. Some limitations appear in the power algorithm using the conventional pi controller, especially in power tracking, error, and quality. In this context, the model reference adaptive controller (MRAC) presents an alternative solution, a robust and efficient controller proposed instead of the pi controllers to control stator powers. Finally, the simulation results confirm that the proposed algorithm could work under hard conditions and demonstrate that the wind energy conversion system (WECS) provides enhanced dynamic responses in transient and steady states and good power quality delivered to the grid.

1. INTRODUCTION

Among several renewable energies, wind energy is considered one of the best promising renewable energy in the world. In the last few years, the installed wind plants worldwide have grown more than 30 % [1,2]. The doubly-fed induction generator (DFIG) is the most useful generator for wind turbine systems due to the various features: maximum power point tracking (MPPT) strategy, which depends on the variable speed operation, decoupled power control, smaller converter prices, and reduced power losses [3,4].

The conventional back-to-back two-level converters are the most used power electronic interface for wind system power generation [5]. However, they need a wide source filter inductor resulting in low reliability, high price, and wide size [6,7]. Nowadays, matrix converters (MC) are more popular due to several interesting gains, like sinusoidal input/output waveforms, bi-directionality power flow, input unity power factor, and the absence of the dc link [6–10]. A direct matrix converter (DMC) can be used to control the DFIG instead of the classical back-to-back converters, as depicted in (Fig. 1). The DMC doesn't require costly energy storage elements, and its implementation scheme is more accessible than that used by two stages power conversion [11].

Recently, vector control (VC) has been the most used control algorithm for a wind turbine-driven DFIG [12,13]. In literature, many control strategies of DFIG have been discussed, such as backstepping control [14,15], fractional order sliding mode control (SMC) [16], high order SMC [17], model predictive direct power control (MPDPC) [18]. Some authors focus their contributions on a simple and robust control based on independent control of rotor currents, named input–output linearizing and decoupling control (I/OLDC) [19], which could work under different operating modes.

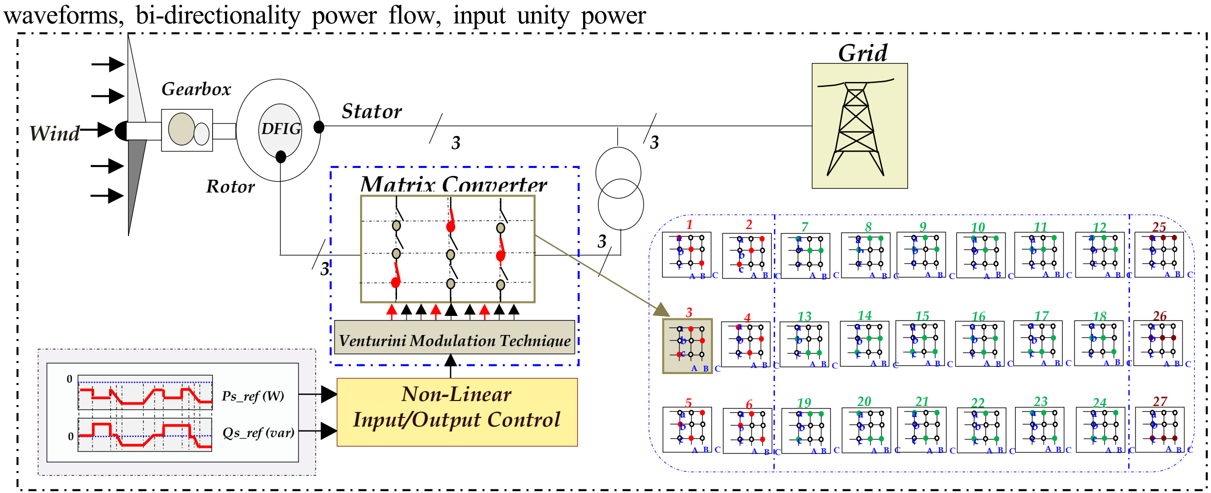

Fig. 1 – WECS based on DFIG-Matrix converter using nonlinear control.

In this work, the nonlinear approach is proposed to control d-q axis rotor currents of the DFIG. Some researchers used

[1,*] LAS Research Laboratory, Department of Electrical Engineering, Ferhat ABBAS Setif-1 University, 19000 Setif, Algeria. Corresponding author: amrane_fayssal@live.fr, amrane_fayssal@univ-setif.dz.
[2] Department of industrial Engineering, University of Khenchela, Algeria. E-mail: chaiba_azeddine@yahoo.fr
[3] Laboratoire d'Electrotechnique et d'Electronique de Puissance de Lille (L2EP), Ecole Centrale de Lille, Lille, France. E-mail : bruno.francois@centralelille.fr.

the PI classical regulators to control the stator powers [20]. Several limitations appear such as: dynamic response, static power error, and delivered power quality. In this context, a robust and adaptive controller named model reference adaptive control (MRAC) [21–24] is applied; instead, the classical PI regulators operate under different modes (sub or super-synchronous mode under random wind speed) to avoid the previous drawbacks.

The main contribution of this paper is the investigation of the improved wind-power algorithm based on nonlinear theory and MRAC adaptive controller (Fig. 1) to guarantee high wind-power performances; different hard tests are proposed.

This paper is structured as follows; firstly, the matrix converter (MC) modeling is presented in section 2. Sections 3 and 4 present a mathematical model of the DFIG and the proposed I/OLDC. In section 5, simulation results are discussed. Finally, the reported work is concluded.

2. MATRIX CONVERTER (MC) MODEL

Three-phase MC connects the three-phase ac voltages on the input side to the three-phase voltages on the output side by a 3*3 Matrix using bidirectional switches. Consequently, there are only $3^3 = 27$ possible states of operation for the switches [25–27]. The output currents and voltages are presented in Table 1. The schematic models of the MC and output voltage waveform (with the zoom) are shown in Fig. 2 and Fig. 3, respectively.

Table 1

27 States of Matrix converter.

Possible States	V_A	V_B	V_C	V_{AB}	V_{BC}	V_{CA}	I_a	I_b	I_c
1	V_a	V_b	V_c	V_{ab}	V_{bc}	V_{ca}	I_A	I_B	I_C
2	V_a	V_c	V_b	$-V_{ca}$	$-V_{bc}$	$-V_{ab}$	I_A	I_C	I_B
3	V_b	V_a	V_c	$-V_{ab}$	$-V_{ca}$	$-V_{bc}$	I_B	I_A	I_C
4	V_b	V_c	V_a	V_{bc}	V_{ca}	V_{ab}	I_C	I_A	I_B
5	V_c	V_a	V_b	V_{ca}	V_{ab}	V_{bc}	I_B	I_C	I_A
6	V_c	V_b	V_a	$-V_{bc}$	$-V_{ab}$	$-V_{ca}$	I_C	I_B	I_A
7	V_a	V_b	V_b	V_{ab}	0	$-V_{ab}$	I_A	$-I_A$	0
8	V_b	V_a	V_a	$-V_{ab}$	0	V_{ab}	$-I_A$	I_A	0
9	V_b	V_c	V_c	V_{bc}	0	$-V_{bc}$	0	I_A	$-I_A$
10	V_c	V_b	V_b	$-V_{bc}$	0	V_{bc}	0	$-I_A$	I_A
11	V_c	V_a	V_a	V_{ca}	0	$-V_{ca}$	$-I_A$	0	I_A
12	V_a	V_c	V_c	$-V_{ca}$	0	V_{ca}	I_A	0	$-I_A$
13	V_b	V_a	V_b	$-V_{ab}$	V_{ab}	0	I_B	$-I_B$	0
14	V_a	V_b	V_a	V_{ab}	$-V_{ab}$	0	$-I_B$	I_B	0
15	V_c	V_b	V_c	$-V_{bc}$	V_{bc}	0	0	I_B	$-I_B$
16	V_b	V_c	V_b	V_{bc}	$-V_{bc}$	0	0	$-I_B$	I_B
17	V_a	V_c	V_a	$-V_{ca}$	V_{ca}	0	$-I_B$	0	I_B
18	V_c	V_a	V_c	V_{ca}	$-V_{ca}$	0	I_B	0	$-I_B$
19	V_b	V_b	V_a	0	$-V_{ab}$	V_{ab}	I_C	$-I_C$	0
20	V_a	V_a	V_b	0	V_{ab}	$-V_{ab}$	$-I_C$	I_C	0
21	V_c	V_c	V_b	0	$-V_{bc}$	V_{bc}	0	I_C	$-I_C$
22	V_b	V_b	V_c	0	V_{bc}	$-V_{bc}$	0	$-I_C$	I_C
23	V_a	V_a	V_c	0	$-V_{ca}$	V_{ca}	$-I_C$	0	I_C
24	V_c	V_c	V_a	0	V_{ca}	$-V_{ca}$	I_C	0	$-I_C$
25	V_a	V_a	V_a	0	0	0	0	0	0
26	V_b	V_b	V_b	0	0	0	0	0	0
27	V_c	V_c	V_c	0	0	0	0	0	0

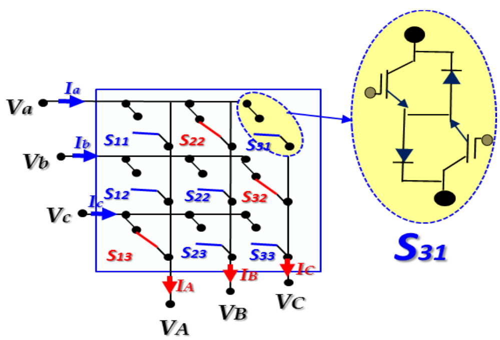

Fig. 2 – Schematic model of Matrix converter (MC).

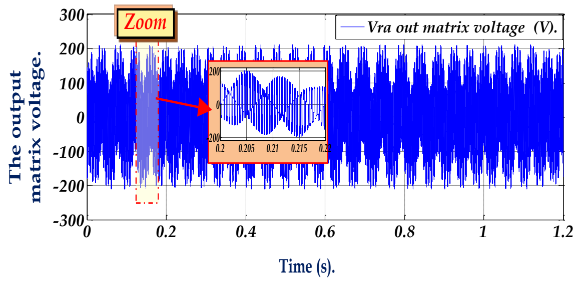

Fig. 3 – The output phase voltage of the Matrix converter.

3. MATHEMATICAL MODEL OF THE DFIG

The mathematical model of the DFIG is presented under the d-q Park reference [1, 21,22]. The stator/rotor voltage and fluxes equations are presented respectively:

$$\begin{cases} Vsd = RsIsd + \dfrac{d}{dt}\phi sd - \omega s\phi sq \\ Vsq = RsIsq + \dfrac{d}{dt}\phi sq - \omega s\phi sd \\ Vrd = RrIrd + \dfrac{d}{dt}\phi rd - (\omega s - \omega)\phi rq \\ Vrq = RrIrq + \dfrac{d}{dt}\phi rq - (\omega s - \omega)\phi rd \end{cases} \tag{1}$$

$$\begin{cases} \phi sd = LsIsd + LmIrd \\ \phi sq = LsIsq + LmIrq \\ \phi rd = LrIrd + LmIsd \\ \phi rq = LrIrd + LmLsq \end{cases} \tag{2}$$

The electromagnetic torque (T_{em}) is presented as follows:

$$\begin{cases} Tem = PLm(IrdIsq - IrqIsd) \\ Tem - Tr = J\dfrac{d}{dt}\Omega + f\Omega \end{cases} \tag{3}$$

where: $\phi sd, \phi sq$ and $\phi rd, \phi rq$ are stator and rotor flux components, respectively, Vsd, Vsq and Vrd, Vrq are stators and rotor voltage components, respectively. Rs, Rr and Ls, Lr are stator and rotor resistances and inductances respectively. Lm is mutual inductance, σ is leakage factor, P is number of pole pairs, ωs is the stator pulsation, ω is the rotor pulsation, f is the friction coefficient, and s is the slip, Tem and Tr: are the electromagnetic and the load torques, J : is total inertia and Ω: is mechanical speed.

The DFIG mathematical model is developed in the synchronous reference frame. This work's d-axis is aligned with the stator flux vector (Fig. 4).

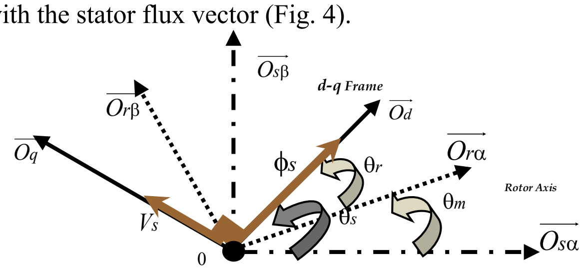

Fig. 4 – Stator flux vector in the d-q reference.

In this work, the stator resistance is neglected. In the steady state, the simplified model is described as follows:

$$Vsd = 0 \text{ and } Vsq = Vs \cong \omega s\phi s \tag{4}$$

$$\phi s = LsIsd + LmIrd \tag{5}$$

$$0 = LsIsq + LmIrq \tag{6}$$

From (5) and (6), the equations of stator/rotor currents:

$$Isd = \frac{\phi s}{Ls} - \frac{Lm}{Ls} Ird \tag{7}$$

$$Isq = -\frac{Lm}{Ls} Irq \tag{8}$$

The DFIG powers are presented as:

$$Ps = VsdIsd + VsqIsq \tag{9}$$

$$Qs = VsqIsd - VsdIsq \tag{10}$$

By applying the d-a reference synchronous frame, the DFIG power equations can be defined:

$$Ps = VsIsq \tag{11}$$

$$Qs = VsIsd \tag{12}$$

Replacing the d-q axis stator currents in expressions (11) and (12), we obtain:

$$\begin{cases} Ps = -Vs\dfrac{Lm}{Ls} Irq \\ Qs = \dfrac{V_s^2}{\omega s Ls} - Vs\dfrac{Lm}{Ls} Ird \end{cases} \tag{13}$$

The rotor quadrature component current I_{rq} controls the stator real power (Ps), and the reactive power is controlled by the direct component I_{rd} as illustrated in the Fig. 5.

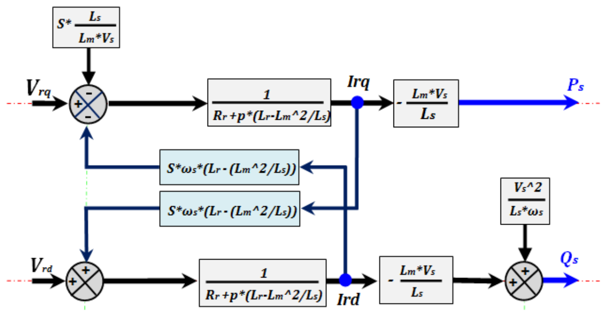

Fig. 5 – The doubly fed induction generator simplified model.

4. PROPOSED INPUT/OUTPUT LINEARIZING AND DECOUPLING CONTROL BASED ON MRAC

Given the system by [19,20] as shown in Fig. 6:

$$\begin{cases} \dot{x} = fn(x) + g.u \\ y = h(x) \end{cases} \tag{14}$$

where x is state vector; u and y are respectively the input and output; fn, g *and* h are smooth vector fields and scalar function respectively.

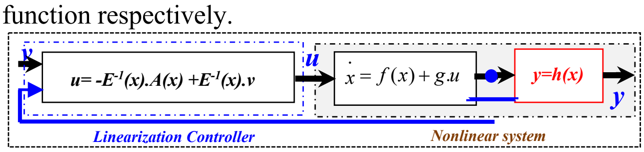

Fig.6 –The input-output linearizing control schematic.

To get the linearization of MIMO system, the y output is differentiated until the inputs appear.

$$\dot{y} = L_f h(x) + L_g(x)u \tag{15}$$

Where: $L_f h(x) = \frac{\partial h}{\partial x}.fn(x)$ and $L_g h(x) = \frac{\partial h}{\partial x} g(x)$; represent Lie derivatives of $h(x)$ with respect to $fn(x)$ and $g(x)$ respectively.

If $L_g h(x) = 0$ then the input u don't appear and the output is differentiated respectively.

$$y^{(r)} = L_f^r h(x) + L_g^{r-1} h(x) u \tag{16}$$

Where "r" is the relative rank of "y". If we perform the above procedure for each input "y_i", we get a total of "m" equations in the above form, which can be written completely as:

$$\begin{bmatrix} y_1^{(r)} \\ \cdots \\ \cdots \\ y_m^{(rm)} \end{bmatrix} = A(x) + E(x) \begin{bmatrix} u_1 \\ \cdots \\ \cdots \\ u_m \end{bmatrix} \tag{17}$$

where the $m*m$ matrix $E(x)$ is defined as:

$$E(x) = \begin{bmatrix} L_{g1} L_f^{r-1} h_1 & \cdots & \cdots & L_{gm} L_f^{r-1} h_1 \\ \cdots & \cdots & \cdots & \cdots \\ \cdots & \cdots & \cdots & \cdots \\ L_{g1} L_f^{rm-1} h_m & \cdots & \cdots & L_{gm} L_f^{rm-1} h_m \end{bmatrix} \tag{18}$$

$$A(x) = \begin{bmatrix} L_f^r h_1 & \cdots & \cdots & L_f^{rm} h_m \end{bmatrix}^T \tag{19}$$

$E(x)$ is the decoupling matrix for the system. If $E(x)$ is nonsingular, then the original input u is controlled by the coordinate transformation:

$$u = -E^{-1}(x)A(x) + E^{-1}(x)v = E^{-1}(x).[v - A(x)] \tag{20}$$

Where $v = \begin{bmatrix} v_1 & \cdots & \cdots & v_m \end{bmatrix}^T$

Substituting (19) into (17) obtains a linear differential relation between the output y and the new input v.

$$\begin{bmatrix} y_1^{(r)} \\ \cdots \\ \cdots \\ y_m^{(rm)} \end{bmatrix} = \begin{bmatrix} v_1 \\ \cdots \\ \cdots \\ v_m \end{bmatrix} \tag{21}$$

According (7) and (8), the direct and quadrature components of the stator and the rotor currents are linearly dependent respectively, thus we choose state vectors of the DFIG as follows:

$$x = \begin{bmatrix} x_1 & x_2 \end{bmatrix}^T = \begin{bmatrix} I_{rd} & I_{rq} \end{bmatrix}^T \tag{22}$$

By substituting (2), (5), (6), (7) and (8) to (1): the rotor voltage d-q components (V_{rd} and V_{rq}) are presented as follows:

$$Vrd = RrIrd + \sigma Lr \frac{d}{dt} Ird - (\omega s - \omega r)\sigma Irq \tag{23}$$

$$Vrq = RrIrq + \sigma \frac{d}{dt} Irq - (\omega s - \omega r)\sigma.LrIrd \tag{24}$$

where: $\sigma = 1 - \frac{L_m^2}{LsLr}$

Arranging (23) and (24) in the form of (14)

$$\frac{d}{dt} Ird = -\frac{Rr}{\sigma Lr} Ird + \frac{1}{Lr}.(\omega s - \omega r).Irq + \frac{Vrq}{\sigma.Lr} \tag{25}$$

$$\frac{d}{dt} Irq = -\frac{Rr}{\sigma}.Irq - (\omega s - \omega r).Lr.Ird + \frac{Vrq}{\sigma} \tag{26}$$

Defining the input of the DFIG system:

$$u = \begin{bmatrix} u_1 & u_2 \end{bmatrix}^T = \begin{bmatrix} V_{rd} & V_{rq} \end{bmatrix}^T \tag{27}$$

From (40) and (41), we have:

$$fn1 = -\frac{Rr}{\sigma.Lr} Ird + \frac{1}{Lr}(\omega s - \omega r)Irq \tag{28}$$

$$fn2 = -\frac{Rr}{\sigma} Irq - Lr(\omega s - \omega r)Ird \tag{29}$$

$$g = \begin{bmatrix} \dfrac{1}{\sigma.Lr} & 0 \\ 0 & \dfrac{1}{\sigma} \end{bmatrix} \tag{30}$$

The selected outputs of the nonlinear system are defined by the stator active (Ps) and reactive (Qs) powers:

$$y=\begin{bmatrix}y_1\\ y_2\end{bmatrix}=\begin{bmatrix}P_s\\ Q_s\end{bmatrix}=\begin{bmatrix}V_{sd}I_{sd}+V_{sq}I_{sq}\\ V_{sq}I_{sd}-V_{sd}I_{sq}\end{bmatrix} \tag{31}$$

From (7), (8) and (31):

$$y_1=\frac{\phi_s}{L_s}V_{sd}-\frac{L_m}{L_s}(V_{sd}I_{rd}-V_{sq}I_{rq}) \tag{32}$$

$$y_2=\frac{\phi_s}{L_s}V_{sq}-\frac{L_m}{L_s}(V_{sq}I_{rd}-V_{sd}I_{rq}) \tag{33}$$

Differentiating (32) and (33) until an input appears:

$$\dot{y}_1=\frac{\dot{V}_{sd}}{L_s}(\phi_s-L_mI_{rd})-\frac{L_m}{L_s}\dot{V}_{sq}I_{rq}-\frac{L_m}{L_s}(V_{sd}f_{n1}-V_{sq}f_{n2}) -\frac{L_mV_{sd}}{\sigma L_sL_r}V_{rd}-\frac{L_mV_{sq}}{\sigma L_s}V_{rq} \tag{34}$$

$$\dot{y}_2=\frac{\dot{V}_{sq}}{L_s}(\phi_s-L_mI_{rd})-\frac{L_m}{L_s}\dot{V}_{sd}I_{rd}-\frac{L_m}{L_s}(V_{sq}f_{n1}-V_{sq}f_{n2}) -\frac{L_mV_{sq}}{\sigma L_sL_r}V_{rd}-\frac{L_mV_{sd}}{\sigma L_s}V_{rq} \tag{35}$$

Rewriting (31) and (35) in the form of (17)

$$\begin{bmatrix}\dot{y}_1\\ \dot{y}_2\end{bmatrix}=A(x)+E(x)\begin{bmatrix}u1\\ u2\end{bmatrix} \tag{36}$$

where:

$$A(x)=\begin{bmatrix}\frac{\dot{V}_{sd}}{L_s}(\phi_s-L_mx1)-\frac{L_m}{L_s}\dot{V}_{sq}x2-\frac{L_m}{L_s}(V_{sd}f_{n1}+V_{sq}f_{n2})\\ \frac{\dot{V}_{sq}}{L_s}(\phi_s-L_mx1)+\frac{L_m}{L_s}\dot{V}_{sd}x2-\frac{L_m}{L_s}(V_{sq}f_{n1}-V_{sq}f_{n2})\end{bmatrix} \tag{37}$$

$$E(x)=\begin{bmatrix}-\frac{L_mV_{sd}}{\sigma L_rL_s} & -\frac{L_mV_{sq}}{\sigma L_s\cdot}\\ -\frac{L_mV_{sq}}{\sigma L_rL_s} & \frac{L_mV_{sd}}{\sigma.L_s}\end{bmatrix} \tag{38}$$

The equivalent scheme of MRAC for adjusting stator active and reactive powers is depicted in Fig. 7. The proposed control is described in detail in Fig. 8.

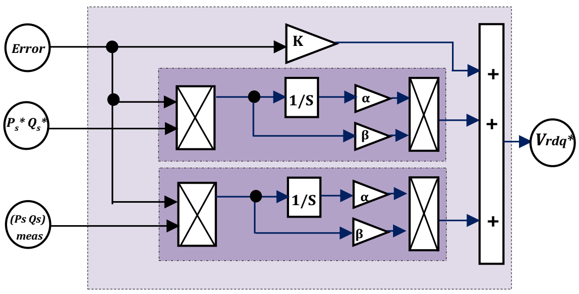

Fig. 7 – The schematic diagram for the proposed MRAC.

Since $E(x)$ is nonsingular, the control scheme is given from (23) and (24) as:

$$\begin{bmatrix}V_{rd}\\ V_{rq}\end{bmatrix}=+E^{-1}(x)\left[-A(x)+\begin{pmatrix}V1\\ V2\end{pmatrix}\right] \tag{39}$$

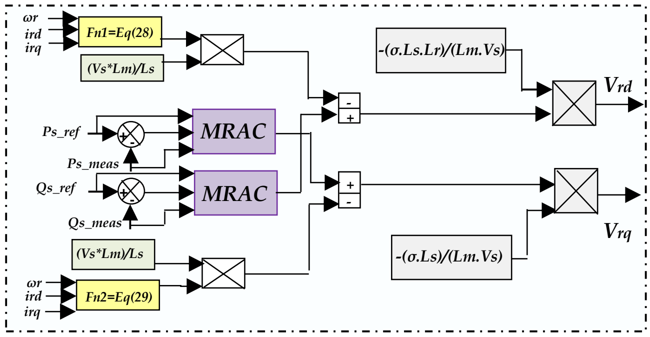

Fig. 8 – Schematic diagram of new input/output linearizing control.

In $A(x)$ and $E(x)$, most components relate to the factors L_m/L_s and σ that are equal to one approximately, and the functions f_{n1} and f_{n2} have no relation with the parameters of the stator windings. Hence, the control law is robust to machine parameter variations.

For the DFIG reference powers, the real reference power Ps* is extracted via the WT's MPPT (maximum power point tracking) strategy according to the wind-speed variation, and the requested reactive power Qs* is defined by the network operator to withstand the network voltage. The model reference adaptive controller (MRAC) performs power tracking. Therefore, the MRAC technique is described below.

In this paper, the studied system is defined as a first-order linear approximation [21-24]:

$$\dot{x}(t)=a.x(t)+b.u(t) \tag{40}$$

where $x(t)$: is the plant state, $u(t)$: is the control signal, a and b are the plant parameters. The control signal is generated from both the state variable and the reference signal $r(t)$, multiplied by the adaptive control gains k and k_r such that:

$$u(t)=k(t)x(t)+kr(t)r(t) \tag{41}$$

where $k(t)$: is the feedback adaptive gain and $k_r(t)$: the feed-forward adaptive gain. The plant is controlled to follow the output from a reference model

$$\dot{x}_m(t)=a_mx_m(t)+b_mr(t) \tag{42}$$

where x_m is the state of the reference model and a_m and b_m are the reference model parameters specified by the controller designer. The object of the *MRAC* algorithm is for $x_e \rightarrow 0$ as $t \rightarrow\infty$, where $x_e=x_m-x$ is the error signal. The dynamics of the system may be rewritten in terms of the error such that

$$\dot{x}_e(t)=a_mx_e(t)+(a-a_m-bk(t))x(t)+ (b_m-bk_r(t))r(t) \tag{43}$$

Using eqs. (41), (42) and (43), it can be seen that for exact matching between the plant and the reference model, the following relations hold

$$k=k^E=\frac{a-a_m}{b} \tag{44}$$

$$k_r=k_r^E=\frac{b_m}{b} \tag{45}$$

where $()^E$ denotes the (constant) Erzberger gains [30].

Equations (44) and (45) can express eq. (43) as:

$$\dot{x}_e(t)=-a_mx_e+b(k^E-k)(x_m-x_e)+b(k^E-k)r \tag{46}$$

For general model reference adaptive control, the adaptive gains are commonly defined in a proportional plus integral formulation

$$k(e,t)=\int_{0}^{t}\alpha\, y_e(Ps\_Qs)^{T}_{meas}\,dt+\beta\, y_e(Ps\_Qs)^{T}_{meas} \quad (47)$$

$$k_r(e,t)=\int_{0}^{t}\alpha\, y_e(Ps\_Qs)^{T}_{ref}\,dt+\beta\, y_e(Ps\_Qs)^{T}_{ref} \quad (48)$$

where α and β are adaptive control weightings representing the adaptive effort. y_e is a scalar weighted function of the error state and its derivatives, $y_e = C_e x_e$ where C_e can be chosen to ensure the stability of the feed-forward block.

In this paper, the proposed MRAC controller also could define as the adaptive controller (generalized definition).

5. SIMULATION RESULTS

The simulation results reported in Figs. 9, 10 presents the electrical behavior of the wind-power generation system under variable wind speed. In this context, the parameters of the DFIG (4.0 kW) and wind turbine (4.5 kW) used in the proposed power algorithm are indicated respectively in Appendix.

Figure 9 shows stator real and reactive powers, respectively. It can be seen clearly that the measured powers track exactly their reference with short response time and neglected overshoot. Also, a perfect decoupled power was noted between 0.05 s and 0.35 s. The stator direct and transversal currents (I_{sd} and I_{sq}), respectively, are shown in Fig .9-c, directly proportional to the reactive and real power (Q_s and P_s). Figure 9-d shows the rotor transversal and direct currents, respectively, which present the inverse curves of stator real and reactive powers. Figure 9-e displays the rotor direct and transversal fluxes, representing the inverse curves of Q_s and P_s, respectively. The tracking error of stator real and reactive powers (Fig. 9-f) when various step changes happen. A low power static error is near: -55 W ≤ ΔPs ≤+55 W and **-55** VAr ≤ ΔQs ≤ **+55** VAr, which means nearly +/-2.5 % from rated power.

The stator currents I_{s_abc} are presented in Fig. 9-g; from the zoom, the sinusoidal form with few ripples (low THD, nearly 01.41 %) can be seen. Figure 9-h depicts the rotor current I_{r_abc}; the perfect sinusoidal form of the 03 phases rotor currents is also noted, without ripples that prove a good tracking of the rotor quadrature and direct currents (abc/dq Park transformation) exactly which the same manner as the stator active and reactive powers which are imposed by the nonlinear input/output power control. So, it is concluded that the rotor quadrature and direct currents are the variable images of the stator's active and reactive powers, respectively. So, the DMC guarantees the bidirectionality of the power flow, the PF unity, and sinusoidal input/output waveforms. In this work, the DFIG works under <1500 rpm (slip $S>0$), which means the sub-synchronous modes, when the rotor absorbs the power from the grid ($Pr=+S*Pn$). In the same manner for the frequencies $f_R=S*f_S$, the rotor frequency is few than the stator frequency ($f_R<f_S$). To confirm the high wind-system performances of the proposed control, robustness tests are applied as shown below (Table 2): the *Ps* and *Qs* are shown in Fig. 10 (a and b, respectively).

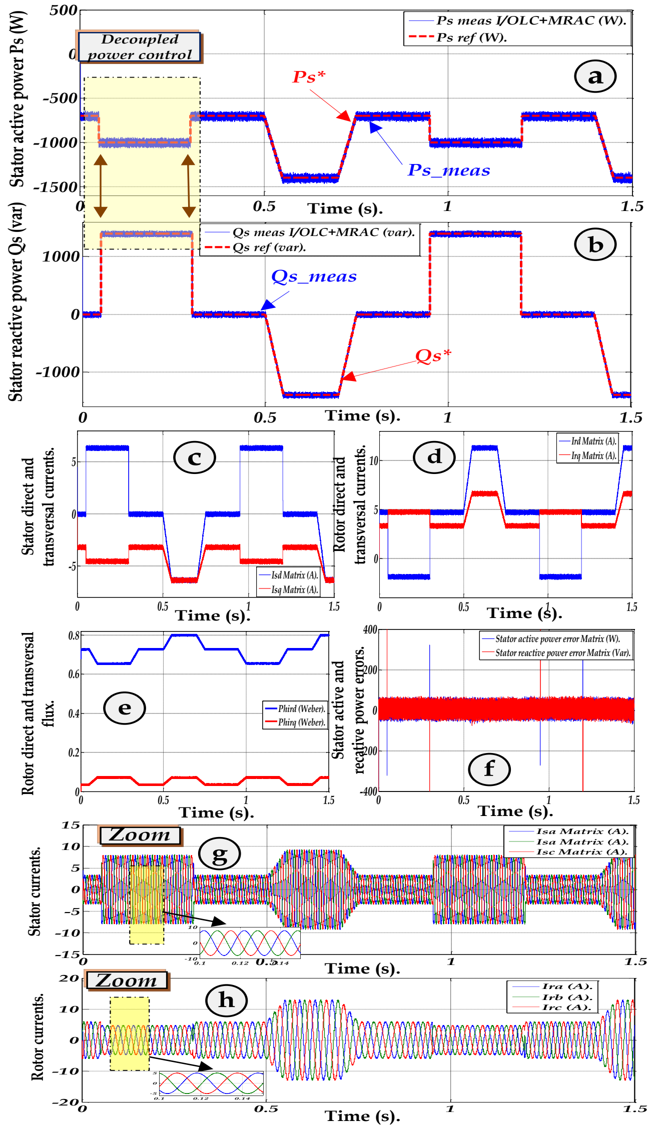

Fig. 9 – (a): Ps(W), (b): Qs(VAr), (c): Isdq(A), (b): Irdq(A), (e): Φrdq(Wb), (f): ΔPs(W) & ΔQs(VAr), (g): Isbac(A), (h): Irabc(A).

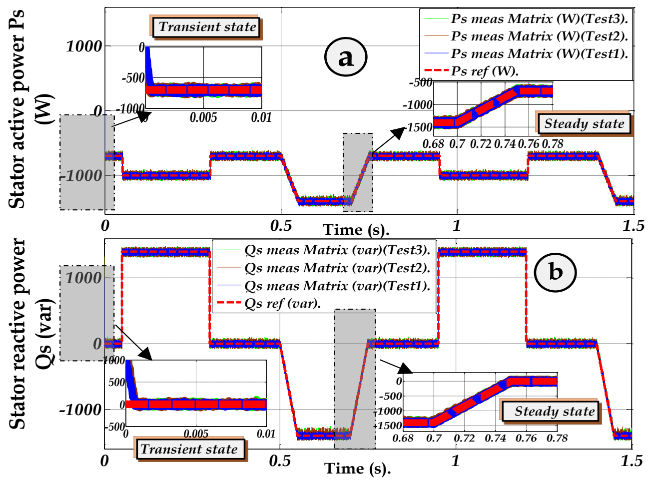

Fig. 10 – Robustness tests with variation of wind system parameters: (a) Ps(W) and (b) Qs VAr).

It is noted that the stator active power (Fig. 10-a) follows exactly its references (Test-1). After robustness tests (Test-2), a good power tracking is noted with few undulations (zoom) with very short response time nearly 0.002 s for both states (transient and steady). After adding

100 % of moment inertia J (Test-3), some ripples are noted, especially between 0.55 s and 0.65 s (due to the sudden) with neglected overshoot, especially in 0.3 s and in 0.95 s. The stator reactive power (Fig. 10-b) also follows exactly its reference (Test-1). After robustness tests (test-2), we note perfect power tracking with a very short response time (< 0.005 s for the transient state). After adding 100 % of J, there can be no overshoot and good power tracking with some ripples between 0.55 s and 0.65 s. The overshoot detection (%), the total harmonic distortion (THD %) of stator currents (from 0.2 s, based on 50 cycles), and THD of rotor currents (from 0.6 s, 20 cycles) and the power errors for the conventional and proposed algorithms are illustrated in Table 3.

Table 2

The robustness tests for the power control.

Test 1:	Without parameters change.
Test 2:	+100% for Rr, -25% for Ls, Lr, and Lm.
Test 3:	+100 % for Rr and J, -25% for Ls, Lr, and Lm.

Table 3

The DFIG power control performances

	Proposed control	Conventional control
The overshoot	<1%	<5%.
THD (%) of I_{sabc}(A)	01.41%	01.42%.
THD (%) of I_{rabc}(A)	12.78%	177.83%.
The power static error: Δ(P, Q) (W, VAR)	+/- 55	+/- 45 .
The response time:	0.000605 s	0.00067 s.

6. **CONCLUSION**

This paper proposes a robust and adaptive DFIG power control for variable speed wind turbines fed by matrix converter. The rotor circuit is fed using a matrix converter (ac/ac), and their IGBTs are controlled via Venturini Technique. In this context, the linearizing power control based on an adaptive controller, "MRAC", offers the best performance, especially in dynamic response and power quality, compared to the conventional vector control. The simulation results obtained using MATLAB/ Simulink® environment demonstrate the feasibility of the proposed algorithm with high wind performances. The experimental validation under dSPACE card of this proposed algorithm presents an excellent perspective for future research works.

APPENDIX

The DFIG parameters [21-22, 28-29]:
Pn=4 kW, Rs = 1.2 Ω, Rr = 1.8 Ω, Ls = 0.1554 H, Lr = 0.1558 H, Lm = 0.15 H, Vs = 220/380 V, P= 2 (pole pairs), Nn= 1440 rpm, f_{DFIG} = 0.00 N.m/s, J = 0.2 kg.m^2.

The Turbine parameters [21,22, 28,29]:
Pn=4.5 kW, P=2 (pole pairs), G= 4.15, J_t = 0.00065 kg.m^2, ft = 0.017 N.m/s, ρ = 1.22 kg/m^3.

ACKNOWLEDGEMENT

This research work falls within the framework of the research project ''PRFU'' under the code: A01L07UN400 120190001, directed by the DGRSDT and the Algerian Ministry of Higher Education and Scientific Research (MESRS).

Received on 3 February 2022

REFERENCES

1. S. Tamalouzt, *Performances of direct reactive power control technique applied to three level-inverter under random behaviour of wind speed*, Rev. Roum. Sci. Techn.– Électrotechn. et Énerg, **64**, 1, pp. 33–38 (2019).
2. Z. Dekali, L. Baghli, A. Boumediene, *Experimental implementation of the maximum power point tracking algorithm for a connected wind turbine emulator*, Rev. Roum. Sci. Techn.– Électrotechn. et Énerg, **66**, 2, pp. 111–117 (2021).
3. H. Nian, Y. Song, *Direct power control of doubly fed induction generator under distorted grid voltage*, IEEE Transactions on Power Electronics, **29**, *2*, p. 894–905 (2014).
4. H. Nian, P. Cheng, Z.Q. Zhu, *Coordinated direct power control of DFIG system without locked loop under unbalanced grid voltage conditions*, IEEE Transactions on Power Electronics, **31**, *4*, pp. 2905–2918 (2016).
5. R. Cárdenas, R. Peña, S. Alepuz, G. Asher, *Overview of Control Systems for the Operation of DFIGs in Wind Energy Applications*, IEEE Transactions on Industrial Electronics, **60**, *7*, pp. 2776–2798 (2013).
6. J.W. Kolar, T. Friedli, J. Rodriguez, P.W. Wheeler, *Review of three-phase PWM ac-ac converter topologies*, IEEE Transactions on Industrial Electronics, **58**, *11*, pp. 4988–5006 (2011).
7. N. Han, B. Zhou, Y. Jiang, X. Qin, J. Lei, Y. Yang, *A novel source current control strategy and its stability analysis for indirect matrix converter*, IEEE Transactions on Power Electronics, **32**, *10*, pp. 8181–8192 (2016).
8. T. Friedli, J.W. Kolar, J. Rodriguez, P.W. Wheeler, *Comparative evaluation of three-phase ac-ac matrix converter and voltage dc-link back-to-back converter systems*, IEEE Transactions on Industrial Electronics, **59**, *12*, pp. 4487–4510 (2012).
9. V. Padhee, A.K. Sahoo, N. Mohan, *Modulation techniques for enhanced reduction in common mode voltage and output voltage distortion in indirect matrix converter*, IEEE Transactions on Power Electronics, **32**, *11*, pp. 8655–8670 (2016).
10. S.K.M. Ahmed, H. Abu-Rub, A. Iqbal, *Multiphase matrix converter topologies and control*, Power Electronics for renewable Energy Systems, Transportation and Industrial Applications, John Wiley & Sons (2014).
11. H.F. Ahmed, H. Cha, A. Khan, J. Kim, J. Cho, *A single-phase buck-boost matrix converter with only six switches and without commutation problem*, IEEE Transactions on Power Electronics, **32**, *2*, pp. 1232–1244 (2017).
12. P. Cheng, H. Nian, C. Wu, Z.Q. Zhu, *Direct stator current vector control strategy of DFIG without phase-locked loop during network unbalance*, IEEE Transactions on Power Electronics, **32**, *1*, pp. 284–297 (2017).
13. P. Cheng, H. Nian, C. Wu, Z.Q. Zhu, *A combined vector and direct power control for DFIG-based wind turbines*, IEEE Transactions on Sustainable Energy, **5**, *3*, pp. 767–775 (2014).
14. P. Xion, D. Sun, *Backstepping-based DPC strategy of a wind turbine-driven DFIG under normal and harmonic grid voltage*, IEEE Transactions on Power Electronics, **31**, *6*, pp. 4216-4225 (2016).
15. B. Bossoufi, M. Karim, A. Lagrioui, M. Taoussi, A. Derouich, *Observer backstepping control of DFIG-Generator for wind turbines variable-speed: FPGA-based implementation*, Renewable Energy, **81**, *3*, pp. 903–917 (2015).
16. Sa. Ebrahimkhani, *Robust fractional order sliding mode control of doubly-fed induction generator (DFIG)-based wind turbines*, ISA Transactions, **63**, *2*, pp. 343–354 (2016).
17. B. Beltran, M. El Hachemi Benbouzid, T. Ahmed-Ali, *Second-order sliding mode control of a doubly fed induction generator driven wind turbine*, IEEE Transactions on Energy Conversion, **27**, *2*, pp. 261–269 (2012).
18. J. Hu, Ji. Zhu, D.G. Dorrell, *Model-predictive direct power control of doubly-fed induction generators under unbalanced grid voltage conditions in wind energy applications*, IET Renewable Power Generation, **8**, *6*, pp. 687–95 (2014).
19. L. Zhang, X. Cai, J. Guo, *Simplified input-output linearizing and decoupling control of wind turbine driven doubly-fed induction generator*, IEEE 6th International Power Electronics and Motion Control Conference, pp. 632–635 (2009).
20. G. Chen, L. Zhang, X. Cai, W. Zhang, C. Yin, *Non-linear control of the doubly fed induction generator by input-output linearizing strategy*, Springer Electronics and Signal Processing, pp. 601–608 (2011).
21. F. Amrane, A. Chaiba, *A novel direct power control for grid-connected doubly fed induction generator based on hybrid artificial*

intelligent control with space vector modulation, Rev. Roum. Sci. Techn.– Électrotechn. et Énerg, **61**, *3*, pp. 263–268 (2016).

22. F. Amrane, A. Chaiba, S. Mekhilef, *High performan-ces of grid-connected DFIG based on direct power control with fixed switching frequency via MPPT strategy using MRAC and neuro-fuzzy control*, Journal of Power Technologies, **96**, *1*, pp. 27–39 (2016).
23. A. Ammar, A. Benakcha, A. Bourek, *Adaptive MRAC-based direct torque control with SVM for sensorless induction motor using adaptive observer*, Springer, The international Journal of Advanced Manufacturing Technology, pp. 1–11 (2016).
24. F. Amrane, A. Chaiba, A, Chebabhi, *Improvement performances of doubly fed induction generator via MPPT strategy using model reference adaptive control based on direct power control with space vector modulation*, Journal of Electrical Engineering, **16**, 3, pp. 218–225 (2016).
25. T, Peng, H, Dan, J. Yang, H. Deng, Q. Zhu, C. Wang, W. Gui, J.M. Guerrero, *Open-switch fault diagnosis and fault tolerant for matrix converter with finite control set-model predictive control*, IEEE Trans. on Industrial Electronics, **63**, *9*, pp. 5953–5963 (2016).
26. B. Metidji, N. Taib, L. Baghli, T. Rekioua, S. Bacha, *Phase current reconstruction using a single current sensor of three-phase ac motors fed by SVM-controlled direct matrix converter*, IEEE Trans. on Industrial Electronics, **60**, 12, pp. 5497–5505 (2013).
27. B. Metidji, N. Taib, L. Baghli, T.k Rekioua, S. Bacha, *Novel single current sensor topology for Venturini controlled direct matrix converters*, IEEE Transactions on Power Electronics, **28**, *7*, pp. 3509–3516 (2013).
28. F. Amrane, A. Chaiba, *Improved indirect power control (IDPC) of wind energy conversion systems (WECS)*, Bentham Science Publishers Pte. Ltd, Singapore, pp. 1–149 (2019).
29. F. Amrane, B. Francois, A. Chaiba, *Experimental investigation of efficient and simple wind-turbine based on DFIG-direct power control using LCL-filter for stand-alone mode*, ISA Transactions, **125**, pp .631–664 (2022).
30. H.K. Khalil, *Nonlinear systems*, Macmillan, New York (1992).
31. S. Róhowicz, A. Zawadzki, *Input-output transformation using the feedback of nonlinear electrical circuits: algorithms and linearization examples*, Mathematical Problems in Engineering, pp. 1–13 (2018).